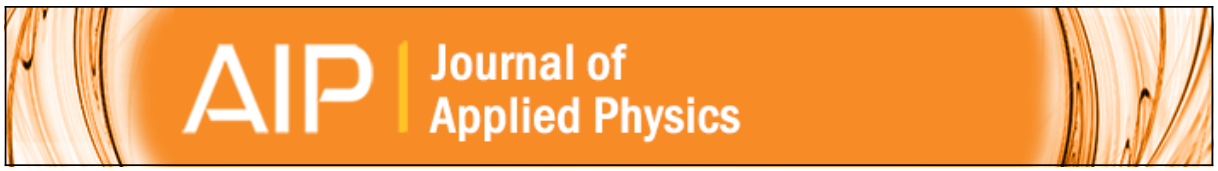

High-pressure Raman scattering of CdO thin films grown by metal-organic vapor phase epitaxy

R. Oliva, J. Ibáñez, L. Artús, R. Cuscó, J. Zúñiga-Pérez, and V. Muñoz-Sanjosé

Citation: Journal of Applied Physics **113**, 053514 (2013); doi: 10.1063/1.4790383
View online: http://dx.doi.org/10.1063/1.4790383
View Table of Contents: http://scitation.aip.org/content/aip/journal/jap/113/5?ver=pdfcov
Published by the AIP Publishing

High-pressure Raman scattering of CdO thin films grown by metal-organic vapor phase epitaxy

R. Oliva,[1] J. Ibáñez,[1] L. Artús,[1] R. Cuscó,[1] J. Zúñiga-Pérez,[2,3] and V. Muñoz-Sanjosé[2]
[1]*Institut Jaume Almera, Consell Superior d'Investigacions Científiques (CSIC), Lluís Solé i Sabarís s.n., 08028 Barcelona, Catalonia, Spain*
[2]*Departament de Física Aplicada i Electromagnetisme, Universitat de València, Dr Moliner 50, València, 46100 Burjassot, Spain*
[3]*Centre de Recherche sur l'Hétéro-Epitaxie et ses Applications, CNRS, Valbonne, France*

(Received 19 November 2012; accepted 22 January 2013; published online 6 February 2013)

We have performed Raman-scattering measurements under high hydrostatic pressure on CdO thin films grown by metal-organic vapor phase epitaxy on sapphire substrates. The pressure dependence of the second-order Raman bands is discussed in terms of *ab initio* lattice-dynamical calculations, which allow us to obtain mode Grüneisen parameters for the zone-center TO and LO modes of CdO. Our experiments and calculations suggest that at low pressures (<4 GPa) the Raman spectra are dominated by second-order modes, while at higher pressures (>4 GPa) the spectra mainly display contributions from disorder-activated first-order modes. © *2013 American Institute of Physics*. [http://dx.doi.org/10.1063/1.4790383]

I. INTRODUCTION

Unintentionally-doped cadmium oxide (CdO) is an *n*-type semiconductor that crystallizes in the rocksalt structure. The direct band-gap energy of intrinsic CdO has recently been shown to lie around 2.2 eV at room temperature.[1,2] CdO exhibits remarkable properties such as low resistivity, high transparency, and high refractive index, which make this compound an excellent candidate for next-generation transparent conducting-oxide layers that could be exploited in photovoltaic cells or flat-panel displays. CdO is also interesting both from applied and fundamental points of view because alloying of CdO with ZnO might allow one to extend the optical emission of ZnO-based structures to longer wavelengths.

Several works have been devoted to investigate the structural and optical properties of CdO.[2–4] However, the vibrational properties of CdO have been comparatively less investigated, which can be partly attributed to the fact that CdO crystallizes in the rocksalt structure and, as a consequence, the first-order Raman modes are symmetry forbidden. Early infrared measurements suggested that the zone-center transverse-optical (TO) and longitudinal-optical (LO) phonon modes of CdO are located at 262 and 523 cm^{-1}, respectively.[5] A first Raman study on polycrystalline CdO showed that the second-order Raman bands of CdO strongly depend on electron density.[6] Recently, we have reported Raman scattering studies on CdO epilayers exhibiting strong second-order modes that were assigned on the basis of *ab initio* calculations of the phonon dispersion curves.[7]

Pressure-induced frequency shifts of the Raman bands strongly depend on the nature (optical or acoustic) and number of phonons involved in the Raman-scattering processes. Thus, the application of high hydrostatic pressures to study the vibrational properties of CdO may provide further information about the assignments of the second-order Raman bands. The high-pressure vibrational properties of rocksalt compounds have been scarcely investigated so far.

Here, we present a high-pressure Raman-scattering investigation of CdO. We use high-quality CdO epilayers grown by metal-organic vapor phase epitaxy (MOVPE) on sapphire. The pressure dependence of the Raman spectra obtained experimentally up to ~16 GPa is discussed in terms of *ab initio* lattice-dynamical calculations at different hydrostatic pressures of the full phonon band structure. From the calculations, bulk modulus and mode Grüneisen parameters for the zone-center TO and LO modes of CdO are obtained. The combined analysis of the experimental results and the calculations allow us to identify the different contributions that dominate the Raman spectrum of CdO at different pressure ranges.

II. EXPERIMENT

High-quality, MOVPE-grown CdO/sapphire epilayers with a thickness of ≈900 nm were used in the present work. Details on the growth conditions and structural properties of these epilayers can be found elsewhere.[8,9] Hall-effect measurements revealed that the as-grown CdO thin films display high *n*-type conductivity, with free-electron densities as high as 1.8×10^{20} cm^{-3} and electron mobilities around 50 $cm^2 V^{-1} s^{-1}$.

For the high-pressure Raman experiments, flakes of CdO/sapphire were loaded into a gasketed membrane-type diamond-anvil cell (DAC). Methanol-ethanol-water (16:3:1) was used as pressure-transmitting medium, and the applied pressure was measured with the ruby fluorescence method.[10] Confocal, unpolarized micro-Raman measurements were performed at room temperature by using the triple subtractive configuration of a Jobin-Yvon T64000 spectrometer equipped with a LN_2-cooled charge coupled device (CCD) detector. The 514.5-nm line of an Ar^+ laser was employed as excitation source. A 50× objective was used to focus the laser beam and to collect the back-scattered light. At ambient pressure, the energy of the absorption edge of the heavily

doped CdO samples used in this work[1] is larger than that of the excitation radiation used to perform the Raman experiments (2.41 eV for the 514.5-nm line of the Ar^+ laser). Thus, it is expected that CdO will remain transparent throughout the high-pressure measurements.

III. RESULTS AND DISCUSSION

A. *Ab initio* lattice-dynamical calculations

Ab initio calculations of the vibrational properties of CdO as a function of hydrostatic pressure were performed with the ABINIT package,[11] which relies on a plane-wave pseudopotential approach to density functional theory (DFT) in the local density approximation (LDA) using the Teter-Pade parametrization of the exchange-correlation functionals.[12] For the calculations, Trouiller-Martins pseudopotentials were used.[13] In the case of the Cd pseudopotential, 4*d* electrons were included as valence states. A $6 \times 6 \times 6$ Monkhorst–Pack *k*-point sampling and a plane wave basis set with an energy cutoff of 60 hartree were considered, giving rise to a convergence of the total energy better than 1 mhartree. The lattice parameter for CdO at ambient pressure obtained after a full structural relaxation of the rocksalt lattice yielded a lattice parameter of $a = 4.6939$ Å, in agreement with reported experimental values (4.6942 Å in Ref. 8). Structural relaxation of the CdO rocksalt lattice as a function of pressure allowed us to determine the bulk modulus at zero pressure ($B_0 = 157.7$ GPa) and its first derivative ($B'_0 = 4.8$). These data agree well with high-pressure structural studies which obtained B_0 values around 150 GPa, with $B'_0 \approx 4$.[14,15]

For the response-function calculations, the dynamical matrices were obtained at different pressure values on a mesh of 28 *k*-points using the density-functional linear-response approach, and the interatomic force constants were generated by a Fourier transformation, which allows the dynamical matrices to be interpolated for arbitrary wave vectors. The full phonon dispersion curves are obtained after diagonalization of the dynamical matrices,[16,17] and one-phonon and two-phonon density of states (2PDOS) are subsequently extracted. To obtain smooth profiles for the density-of-states curves, a Gaussian-like smearing technique was employed.

Figure 1 shows the phonon dispersion curves and PDOS of CdO at two different pressures, $P = 0$ and $P = 10$ GPa. The corresponding PDOS is plotted in the right panel of Fig. 1. As can be seen in the figure, the lattice-dynamical calculations predict a very small frequency gap at ambient pressure between the acoustic and optical branches. At $P = 10$ GPa the calculations predict a considerable opening of the phonon gap, which is particularly evident at the L point. On the other hand, the calculated PDOS exhibits an overall upward frequency shift with increasing pressure. From the pressure-induced frequency shifts of the zone-center TO phonon (266.5 cm^{-1}) and the LO phonon (429.6 cm^{-1}), the mode Grüneisen parameters, γ_i, for these two modes were obtained. For the TO(Γ) mode, we obtain a pressure coefficient of 4.9 cm^{-1}/GPa ($\gamma_{TO} = 2.90$). For the LO(Γ) mode, in spite of the similar pressure coefficient (4.6 cm^{-1}/GPa), the calculated mode Grüneisen parameter is much lower

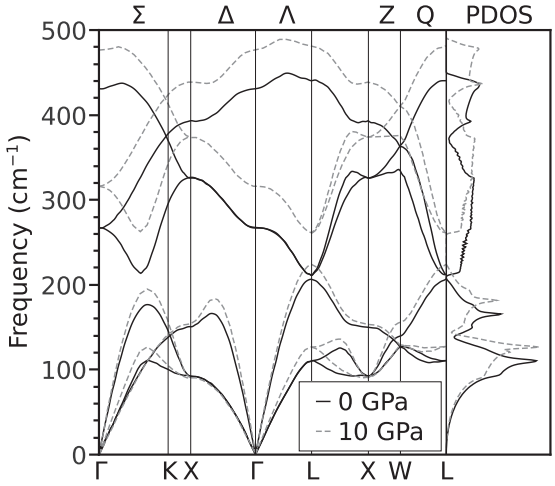

FIG. 1. Calculated phonon dispersion curves at 0 GPa (solid line) and 10 GPa (dashed line). The corresponding one-phonon density of states for both pressure values is shown on the right panel of the figure.

($\gamma_{LO} = 1.69$), which is a consequence of the large TO-LO splitting in CdO. These data can be found in Table I. Note, however, that the LDA calculations tend to fail for the calculation of LO frequencies. The intrinsic limitations of the calculations based on the LDA functional, which can be particularly important in strongly correlated systems such as transition-metal oxides, yield a substantial overestimation of the high-frequency dielectric constant, giving rise to large underestimations of the LO-TO splitting.

The Raman spectrum of rocksalt CdO and its pressure dependence are expected to reflect the 2PDOS. Figure 2 shows the calculated two-phonon sum and difference 2PDOS curves for $P = 0$ and 10 GPa. While the contribution of different modes at ambient pressure extends below 400 cm^{-1} and dominates the low-frequency spectral range (<150 cm^{-1}), the sum 2PDOS extends over a wide frequency range, from 200 cm^{-1} up to 900 cm^{-1}. Upon increasing pressure, the DFT calculations predict sizable upward frequency shifts for most of the features with high-density of states that appear in both the sum and difference 2PDOS. Only in the 50–80 cm^{-1} range the difference 2PDOS exhibits a maximum that barely shifts with pressure, and which can be attributed to LA-TA or LO-TO difference modes as will be discussed below. In the next sections, the calculated pressure coefficients will be used to assess the assignment of the second-order Raman bands that appear in the Raman spectrum of CdO.

B. High-pressure Raman spectrum of CdO

Figure 3 shows Raman spectra of CdO at different hydrostatic pressure values. A smooth background signal attributed to diffused light within the DAC was subtracted from the Raman spectra. Several broad features are observed

TABLE I. Calculated pressure coefficients and mode Grüneisen parameters for the zone-center LO and TO modes of CdO.

CdO phonons	dω/dP (cm^{-1}/GPa)	Grüneisen parameter
TO (Γ)	4.9	2.90
LO (Γ)	4.6	1.69

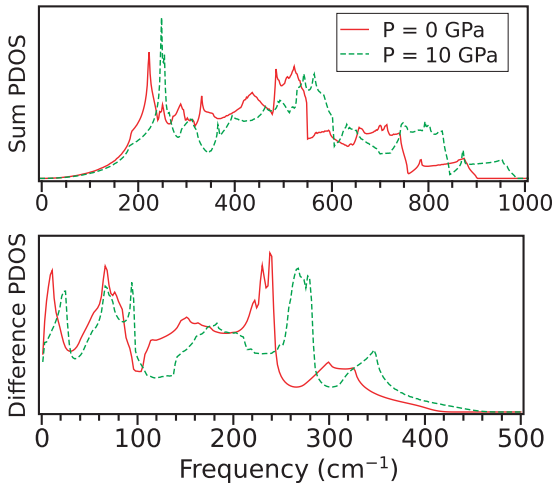

FIG. 2. Sum (upper panel) and difference two-phonon density of states at pressures values of 0 GPa (solid line) and 10 GPa (dashed line).

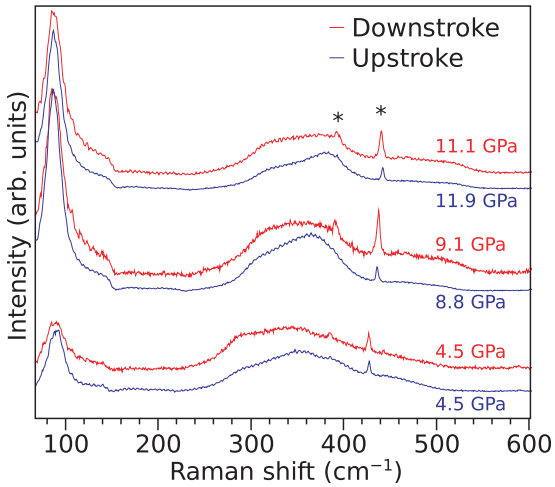

FIG. 4. Comparison of Raman spectra of CdO at different hydrostatic pressures obtained in the upstroke and downstroke cycles. Peaks from the sapphire substrate have been marked with an asterisk.

in the Raman spectra of Fig. 3. The different bands have been labeled from A to F. The A_{1g} mode ($\omega \approx 420\,\text{cm}^{-1}$ at $P = 0$) and E_g mode ($\omega \approx 750\,\text{cm}^{-1}$ at $P = 0$) of sapphire are also visible in all the spectra, showing that the CdO layers remain mostly transparent throughout the whole experiment. The obtained pressure dependence of these two modes (not shown) was in good agreement with previous Raman scattering measurements on bulk sapphire.[18] In Fig. 3, the peaks from sapphire are marked with an asterisk. In some of the spectra, weak Raman features corresponding to the methanol-ethanol-water (16:3:1) mixture can also be distinguished in the high-frequency spectral range at ≈880, 1033, and 1065 cm^{-1}.

The reproducibility of these experiments was checked by repeating the high-pressure Raman measurements on a second CdO/sapphire flake. The results thus obtained were highly coincident with the first set of experiments, with equivalent number and shape of Raman features as a function of pressure. As can be seen in Fig. 4, the high-pressure Raman spectra are also well reproduced in the downstroke cycle. In particular, as can be seen in the figure, the intensity ratio between the low-frequency (A) and medium-frequency (B to E) features is clearly recovered after the downstroke cycle, which suggests that the crystal lattice of CdO has not suffered any irreversible damage during the upstroke cycle.

In the low frequency region, a broad feature labeled A_1 shows up in the spectra acquired at low hydrostatic pressures (Fig. 3). This band, which barely shifts with increasing pressure, can be distinguished from the A_2 peak, which displays a strong intensity enhancement and a very small negative pressure coefficient. As can be seen in Fig. 5, the zero pressure frequency extrapolated for these two peaks is different, which suggests that they are originated by different Raman modes.

In the 200–500 cm^{-1} range, a broad band is observed at ambient pressure.[7] This band can be decomposed in 4 contributions, which in Fig. 3 are labeled as B_1, C_1, D, and E. The pressure behavior of the features is plotted in Fig. 5. Feature B_1, located at 265 cm^{-1} at $P = 0$, is the sharpest feature in the Raman spectrum of CdO at ambient pressure and was tentatively assigned as a 2TA(L) mode in Ref. 7. With

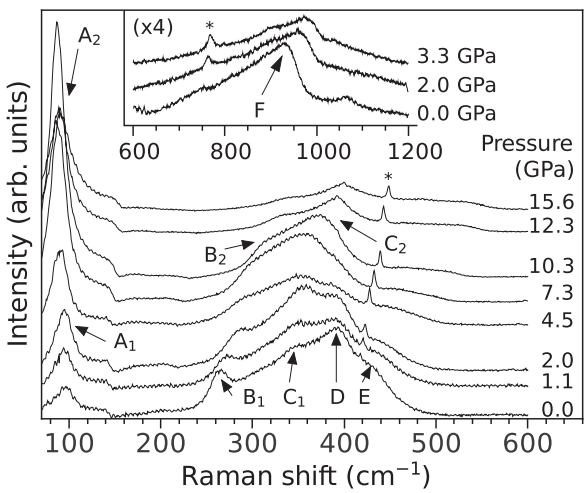

FIG. 3. Raman spectra of CdO at different hydrostatic pressures. The inset shows the Raman signal observed in the high-frequency region of the spectrum. Peaks from the sapphire substrate have been marked with an asterisk.

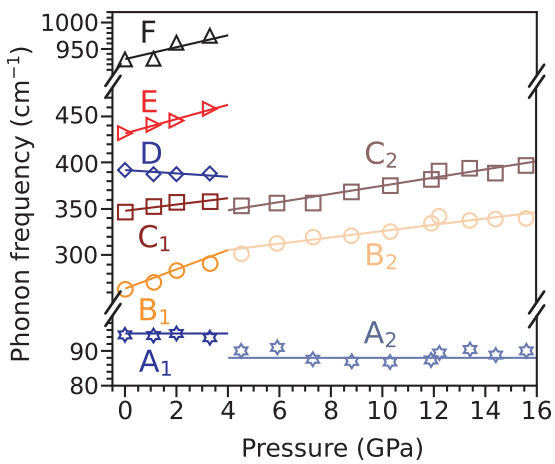

FIG. 5. Phonon frequency of the different features observed in the Raman spectrum of CdO as a function of hydrostatic pressure.

increasing P, this feature displays a sizable upward frequency shift of $8.5 \pm 2\,cm^{-1}$/GPa and a clear loss of intensity. This high pressure coefficient already indicates that optical modes probably contribute to this feature, as will be discussed below. Above 4.5 GPa this band has completely smeared out. Similarly, features D and E rapidly weaken and disappear at intermediate pressures. On the contrary, feature C_1 seems to gain intensity in relation to the rest of features in the low pressure regime, from ambient pressure up to 2 GPa. At higher pressure values this band smears out completely. In the same frequency region, a new feature (C_2) emerges for $P > 5$ GPa. While the pressure behavior exhibited by bands C_1, D, and E is fairly weak, this feature exhibits a relatively large blueshift of around $4.4 \pm 1\,cm^{-1}$/GPa with increasing pressure. Similarly, above 5 GPa a broad feature emerges on the low-frequency shoulder around 300 cm^{-1} (feature B_2). Although the large width of band B_2 makes it very difficult to accurately determine its pressure coefficient, this feature displays a sizable blueshift with increasing P, not lower than $3.5\,cm^{-1}$/GPa. As will be discussed below, the appearance of bands B_2 and C_2 might be related to disorder activated TO modes.

C. Assignment of the Raman modes

In order to assign the different features (A to F) observed experimentally, we have compared their pressure behavior with that of first-order and second-order (sum and difference) phonon modes at high-symmetry points of the Brillouin zone obtained with *ab initio* lattice-dynamical calculations. In Table II, we show a tentative assignment performed for some of these bands together with the pressure coefficient measured experimentally (see Fig. 5) and the corresponding frequency extrapolated to $P = 0$ GPa. For comparison, the calculated pressure coefficient and zero-pressure frequency of the assigned modes can be found in the table in parentheses. Next, we proceed to discuss on the assignments performed for the observed features:

(i) The lattice dynamical calculations reveal that the frequency and pressure behavior of LA-TA difference modes around the L point are very similar to those of feature A_1. On the other hand, the temperature behavior of this band indicates that it arises from a phonon-difference second-order mode.[7] Thus, this band can be assigned to a LA-TA(L) mode.

(ii) Regarding the A_2 band observed at higher pressures in the same frequency range as feature A_1, we first note that in the 90–120 cm^{-1} region the calculated one-phonon PDOS (Fig. 1) exhibits sharp features arising from TA modes. On the other hand, and bearing in mind the large errors expected for the LDA calculations of the LO frequencies, the *ab initio* calculations reveal that LO-TO modes as well as LA-TA modes may also be expected in this spectral region. We conclude that the A_2 band most probably reflects the large difference PDOS at different points of the Brillouin zone, although it cannot be ruled out that this feature displays an important contribution from disorder-activated transverse acoustic (DATA) modes.

(iii) Our measurements reveal that the B_1 peak displays a large pressure coefficient, as high as $8.5 \pm 2\,cm^{-1}$/GPa. This large value suggests that this feature cannot be attributed to first order modes or to combination modes involving only acoustic phonons, as for instance a 2TA combination. Here we tentatively assign this band to a TA+TO mode at the L point, for which the lattice-dynamical calculations predict a relatively large pressure coefficient ($6.6\,cm^{-1}$/GPa, see Table I). Although this value is sizably lower than the experimental one, it should be noted that the error of the measurement is large as the B_1 band rapidly smears out with increasing pressure (see Fig. 3).

(iv) As discussed in Ref. 7, features C_1, D, and E arise from second-order combinations in the region of 330–450 cm^{-1}. The pressure behavior of bands C_1 and E, plotted in Fig. 5, is compatible with the expected qualitative behavior of second-order modes in this spectral region (see Fig. 2). In the case of band D, however, a negative pressure coefficient is observed (not included in Table II). We speculate that this behavior and also the pressure-induced shifts displayed by features C_1 and E is the consequence of strong band overlapping of a large number of second-order combinations around this particular frequency region, giving rise to the observed pressure dependence of the observed features.

(v) The broad B_2 and C_2 bands emerge at pressures higher than ~4 GPa and display sizable pressure coefficients which cannot be accurately measured because

TABLE II. Experimental pressure coefficient (third column) and phonon frequency at zero pressure (second column) as obtained from the data of Fig. 5 for the different features that appear in the high-pressure Raman spectra of CdO. In parentheses, theoretical values obtained with *ab initio* calculations for first- and second-order phonon modes at different high-symmetry points of the Brillouin zone. The last column displays the phonon mode considered for such calculations.

Feature	Zero pressure frequency (cm^{-1})	$d\omega/dP$ (cm^{-1}/GPa)	Pressure range (GPa)	Phonon mode
A_1	95 ± 1 (95.7)	0.0 ± 0.5 (0.1)	0–4	LA-TA(L)
A_2	88 ± 1 (83.4, 93.1)	0.0 ± 0.5 (−0.4,−0.2)	5–16	LO-LO(K),TA(X)
B_1	264 ± 2 (322.7)	8.5 ± 2 (6.6)	0–4	TA+TO(L)
C_1, E	300–450	3.5 ± 1	0–4	Second orders
B_2	292 ± 2 (291.3)	>3.5 (4.8)	5–16	TO(K)
C_2	331 (325.8, 333.6)	4.4 ± 1 (4.8, 4.3)	5–16	TO(X), TO(W)
F	930 ± 3 (859.2, 882.4)	11 ± 1 (9.2, 8.0)	0–4	2LO(Γ), 2LO(L)

of the large width of these two bands. According to our lattice-dynamical calculations, the pressure-induced shift of these bands is compatible with the pressure behavior of TO modes (see Table II). We speculate that this spectral region is dominated at low pressure values (<4 GPa) by second-order modes, while at higher pressures (>4 GPa) it is dominated by TO modes, which might be activated by pressure-induced disorder.

(vi) As occurs with the rest of second-order bands, feature F vanishes at pressures higher than 4 GPa. This band, attributed in Ref. 7 to second-order optical modes, exhibits a high pressure coefficient of $11 \pm 1\,cm^{-1}$/GPa. This result confirms that this band corresponds to longitudinal optical second-order modes, probably arising from the L or Γ points. Note that, as already mentioned, the difference between the experimental and calculated data for this band (see Table II) can be attributed to the typical underestimation of the TO-LO splitting of LDA calculations. In any case, the agreement between our experimental pressure coefficients and the calculations is better than 8%, thus confirming that feature F arises from 2LO combinations. The intensity loss observed for this band at higher pressures supports the previous discussion, i.e., that second-order modes (disorder-activated first-order modes) tend to disappear (dominate) at higher applied pressures.

IV. CONCLUSION

We have performed Raman-scattering measurements of CdO at high hydrostatic pressures. The experimental results have been analyzed in terms of *ab initio* lattice-dynamical calculations of the full phonon band structure of CdO as a function of pressure. All features in the Raman spectra of CdO at pressures below 4 GPa are assigned to second-order modes. In contrast, our experimental results and calculations suggest that at higher pressures the Raman spectrum is dominated by disorder-activated first order modes. From the lattice-dynamical calculations, Grüneisen parameters of 2.90 and 1.69 were obtained for the zone-center TO and LO modes, respectively.

ACKNOWLEDGMENTS

This work was supported by the Spanish Government under projects MAT2010-16116 and TEC2011-28076-C02-02 and by Generalitat Valenciana under projects Prometeo/2011-035 and ISIC/2012/008.

[1]P. H. Jefferson, S. A. Hatfield, T. D. Veal, P. D. C. King, C. F. McConville, J. Zuniga-Perez, and V. Munoz-Sanjose, Appl. Phys. Lett. **92**, 022101 (2008).
[2]A. Segura, J. F. Sánchez-Royo, B. García-Domene, and G. Almonacid, Appl. Phys. Lett. **99**, 151907 (2011).
[3]S. K. V. Farahani, T. D. Veal, P. D. C. King, J. Zúñiga-Pérez, V. Muñoz-Sanjosé, and C. F. McConville, J. Appl. Phys. **109**, 073712 (2011).
[4]S. G. Choi, J. Zúñiga-Pérez, V. Muñoz-Sanjosé, A. G. Norman, C. L. Perkins, and D. H. Levi, J. Vac. Sci. Technol. B **28**, 1120 (2010).
[5]H. Finkenrath, N. Uhle, and W. Waidelich, Solid State Commun. **7**, 11 (1969).
[6]G. Schaack and N. Uhle, Solid State Commun. **19**, 315 (1976).
[7]R. Cuscó, J. Ibáñez, N. Domenech-Amador, L. Artús, J. Zúñiga-Pérez, and V. Muñoz-Sanjosé, J. Appl. Phys. **107**, 063519 (2010).
[8]J. Zúñiga-Pérez, C. Munuera, C. Ocal, and V. Muñoz-Sanjosé, J. Cryst. Growth **271**, 223 (2004).
[9]J. Zuñiga-Pérez, C. Martínez-Tomás, and V. Muñoz-Sanjosé, Phys. Status Solidi C **2**, 1233 (2005).
[10]G. J. Piermarini, S. Block, J. D. Barnett, and R. A. Forman, J. Appl. Phys. **46**, 2774 (1975).
[11]X. Gonze *et al.*, Comput. Phys. Commun. **180**, 2582 (2009).
[12]S. Goedecker, M. Teter, and J. Hutter, Phys. Rev. B **54**, 1703 (1996).
[13]N. Troullier and J. L. Martins, Phys. Rev. B **43**, 1993 (1991).
[14]H. Z. Liu, H. K. Mao, M. Somayazulu, Y. Ding, Y. Meng, and D. Häusermann, Phys. Rev. B **70**, 094114 (2004).
[15]J. Zhang, Phys. Chem. Miner. **26**, 644 (1999).
[16]X. Gonze and C. Lee, Phys. Rev. B **55**, 10355 (1997).
[17]S. Baroni, S. de Gironcoli, A. Dal Corso, and P. Giannozzi, Rev. Mod. Phys. **73**, 515 (2001).
[18]G. H. Watson, W. B. Daniels, and C. S. Wang, J. Appl. Phys. **52**, 956 (1981).